Vortex Formations and Its Associated Surges in a Sunspot Light Bridge

Heesu Yang[1], Eun-Kyung Lim[1], Haruhisa Iijima[2], Vasyl Yurchyshyn[3], Kyung-Suk Cho[1], Jeongwoo Lee[4],
Brigitte Schmieder[1,5], Yeon-Han Kim[1], Sujin Kim[1], and Su-Chan Bong[1]

[1] Korea Astronomy & Space Science Institute, Daejeon 34055, Republic of Korea; hsyang@kasi.re.kr
[2] Division for Integrated Studies, Institute for Space-Earth Environmental Research, Nagoya University, Japan
[3] Big Bear Solar Observatory, New Jersey Institute of Technology, 40386 North Shore Lane, Big Bear City, CA 92314-9672, USA
[4] Institute of Space Sciences, Shandong University, Weihai, Shandong 264209, People's Republic of China
[5] Observatoire de Paris, LESIA, F-92190 Meudon, France

Abstract

We report on the successive occurrence of $0\rlap{.}''5$ wide photospheric vortices with strong transverse shear flows at the edge of a sunspot light bridge (LB), and the subsequent ejection of chromospheric surges observed using a Visible Inteferometry Spectrograph, a broadband TiO filter, and a Near InfRared Imaging Spectrograph of the Goode Solar Telescope operating at Big Bear Solar Observatory. The Hα surges ejected at the location of the vortices often appeared in a hollow cylindrical structure. We also observed quasi-periodic vortex-associated bright Hα plasma blobs moving upward with a speed of up to $4 \,\mathrm{km \, s^{-1}}$. In view of the strong shear flow at the edge of the LB, it is likely that the vortices form under the Kelvin–Helmholtz instability. The surges may result from either the magnetic tension generated after magnetic reconnection or an acoustic impulse of a fast photospheric transverse flow. Otherwise, the surges could also be associated with Alfvénic waves, in which case their origin could be torsional magnetic fields generated in the process of the vortex formation.

Key words: instabilities – Sun: activity – Sun: chromosphere – Sun: photosphere

Supporting material: animation

1. Introduction

Hα surges, which are jets of cool chromospheric plasma, are protruding into the solar corona 10–100 Mm above the photosphere. They are observed in conjunction with hot jets seen in the X-ray (Schmieder et al. 1993; Canfield et al. 1996); however, the cool and hot components of the jets are not strictly cospatial (Alexander & Fletcher 1999; Chae et al. 1999; Jiang et al. 2007). Surges commonly occur in regions of an emerging magnetic flux (Kurokawa & Kawai 1993), above sunspot light bridges (LBs; Roy 1973; Asai et al. 2001), or satellite sunspots (Rust 1968; Canfield et al. 1996; Shimojo et al. 1998; Shimizu et al. 2002). On a smaller scale, they are often associated with sudden photospheric magnetic field changes resulting from various activities such as moving magnetic features or emerging bipoles (Yang et al. 2013, 2016) showing periodic pulsating behavior and following the same curved trajectory with a life time of 10–20 minutes. Some surges appear to consist of a bundle of multiple shock features, indicating that they may be multithreaded (Yang et al. 2014).

The driving mechanisms of Hα surges have been widely studied both theoretically and numerically. The most promising model of surge formation is energy release via magnetic reconnection in the chromosphere (Heyvaerts et al. 1977; Canfield et al. 1996; Wang 1998; Chae et al. 1999; Shimizu et al. 2009). But the details of the acceleration mechanism of chromospheric plasma is still elusive. The cool chromospheric plasma can be accelerated upward by the magnetic tension of reconnected field lines, the so-called slingshot effect (Yokoyama & Shibata 1995; Nishizuka et al. 2008), or by

slow mode shock waves colliding with the transition region (Shibata et al. 1982; Suematsu et al. 1982; Takasao et al. 2013). The slow mode shock waves can develop from acoustic waves in a stratified medium when they are triggered by magnetic reconnection (Shibata et al. 1982; Suematsu et al. 1982). The evaporation outflow can also generate shock waves that are capable of accelerating plasma (Shimojo & Shibata 2000). The untwisting motion of reconnected magnetic field lines that were originally twisted at the time of emergence, can accelerate plasma along open field lines as well (Shibata & Uchida 1986; Schmieder et al. 1995; Pariat et al. 2009, 2010, 2015, 2016; Moreno-Insertis & Galsgaard 2013).

Another possible driver is the MHD waves from the photosphere. The shocks, which are formed from magnetoacoustic waves caused by leakage of p-mode oscillations (Suematsu 1990; Tian et al. 2018) can squeeze out the plasma inside a flux tube along the guide magnetic field lines. The Alfvén waves driven by the photospheric convective motion also generate shocks by increasing pressure at the magnetically concentrated region (Hollweg et al. 1982; Iijima & Yokoyama 2017). These models can explain the quasi-periodic property of chromospheric jets as a modulation of periodic waves in the photosphere.

One of the most interesting features of a surge is its rotation during ascending and descending motions (Canfield et al. 1996; Cho et al. 2019). In fact, the rotational motion of jets appears to be common and it has been reported that they can be detected in 10%–14% of the X-ray jets (Shimojo et al. 1996; Savcheva et al. 2009), up to 30% of the EUV jets in SECCHI/*STEREO* observations (Nisticò et al. 2009), and most of the AIA 304 Å jets (Moore et al. 2013). The fraction of jets exhibiting rotational motions is likely to increase for cooler jets (Pariat et al. 2016).

This rotational motion has been modeled as a redistribution of the stored twist. Many previous studies have suggested that magnetic reconnection between emerging twisted magnetic fields and preexisting open fields can produce the twisted motion observed in jets (Canfield et al. 1996; Pariat et al. 2009, 2010, 2015). The rotational motion may also be caused by the photospheric turbulence (Curdt et al. 2012; Kitiashvili et al. 2013). The rotational motions of spicules or tornados observed in solar quiet regions have been explained as the magnetic field braiding and twisting as a result of photospheric convective motion (Wedemeyer-Böhm & Rouppe van der Voort 2009; Wedemeyer-Böhm et al. 2012; Iijima & Yokoyama 2017). Fast photospheric transverse motions with convective downflows at the roots of surges (Yang et al. 2013, 2014) may cause the Kelvin–Helmholtz instability (KHI) or the swirling motion (sometimes called the bathtub effect, Nordlund 1985) to develop, which plays a crucial role in rotating the jets.

In this paper, we present high-resolution observations of surge ejection observed using the Goode Solar Telescope (GST) at Big Bear Solar Observatory (BBSO). Its unprecedented spatial resolution allowed us to find photospheric vortices of rare clarity in TiO images. Accordingly, we mainly investigate whether vortex formation is related to surge ejection in order to find new clues to the origin of the rotation of the surges. We start by describing the observation setup and data reduction in Section 2. We present major observational findings in Section 3, and finally discuss them in Section 4.

2. Observation

We observed the NOAA active region (AR) 11542 located near the disk center (115″, 245″) in the heliocentric coordinate on 2016 May 5. The observations were performed using the Visible Imaging Spectrometer (VIS), the Near InfraRed Imaging Spectropolarimeter (NIRIS), and the Broadband Filter Imager (BFI) installed at the GST operating at BBSO. The VIS provides chromospheric data using Fabry–Pérot etalon that allowed us to set the 0.07 Å bandpass at stepped positions of -1.2, -1.0, -0.8, -0.4, 0.0, $+0.4$, $+0.8$, $+1.0$, $+1.2$ Å measured from the Hα line center. The data used in this study were taken at -0.8, -0.4, 0, $+0.4$, $+0.8$ Å at two second intervals between each wavelength position. The speckle reconstruction technique was applied to the data using the Kiepenheuer-Institute Speckle Interferometry Package (Wöger et al. 2008).

The BFI collected photospheric images at TiO 7057 Å, with a pixel scale of 0.″0375. Speckle reconstruction was also applied to the data to obtain the diffraction-limited resolution of 0.″11.

The NIRIS offers high-resolution spectroscopic and polarimetric imaging data of the photosphere. The field of view (FOV) of NIRIS is 85″ × 42.″5, and the cadence was set to be about 194 s. We used the Fe I 15650 Å doublet that has already proven to be the most sensitive to the Zeeman effect in this spectral range (Cao et al. 2012).

3. Results

NOAA AR 11542 was emerging when it first appeared at the east solar limb. Two sunspots collided with each other before the observing run started. During the sunspot approach, an LB was formed between them, which crossed the sunspot from east to west and became thinner with time. After the observing run the two sunspots eventually merged so that the LB disappeared by the time the sunspots reached the west limb.

Figure 1 displays the overall structure of AR 11542 as it appeared in the Hα and TiO images. At the moment of observations, the LB had a well-defined boundary with the umbra. This LB can be classified as a filamentary LB following the classification of Sobotka (1997). It showed multiple lanes running parallel to the LB axis rather than a single central dark lane with short and narrow dark and bright lanes branching out of that central dark lane (Lites et al. 2004; Guglielmino et al. 2017). These multiple lanes inside the LB are similar to the filamentary structures of a sunspot penumbra or an orphan penumbra, which are likely to be formed by flux ropes trapped in the photosphere by strong overlying preexisting fields (Lim et al. 2013; Zuccarello et al. 2014).

The filamentary structure of the LB is distinct from several other LBs identified in the southern part of the umbra, which consisted of round convection-cells characteristic of a granular- and segmented-LB (Thomas & Weiss 2004; Lagg et al. 2014). In this paper, we concentrate on the dynamic structures at the edge of the filamentary-LB extending in the east–west direction.

Many chromospheric surges originated above the LB. Surges at the east end of it were associated with abrupt chromospheric brightenings occurring at their footpoints. The surges are well-documented in the animation associated with Figure 1. The apparent length of the surges at the east end was about 5–15 Mm, which is longer than the 5 Mm length of other surges that occurred at the central and the west side of the LB. These 5–15 Mm length surges and associated phenomena are similar to the LB jets observed by Toriumi et al. (2015b). Details of the surges and associated magnetic reconnection were studied by E. K. Lim et al. (2019, in preparation).

This paper focuses on the comparatively short surges at the central and the west side of the LB. The surges first appeared blueshifted in the early phase of their development, and then they gradually evolved to become redshifted. The redshifted stage of the surges lasted longer than the blueshifted stage. They were ejected from photospheric vortices (black arrow in Figure 1(c)) seen in the TiO images projecting from the LB (black arrows in Figures 1(b) and (d)) into the umbral region.

3.1. Photospheric Vortices

Figure 2 shows photospheric horizontal motions in the LB. The flow velocity vectors were obtained by applying the nonlinear affine velocity estimate method (NAVE; Chae & Sakurai 2008) to two TiO images taken 75 s apart. The flow map was defined on a 5 × 5 pixel grid using a window size of 10 pixels and plotted only for the grid points associated with the LB.

The average speed in the LB was found to be about 0.7 km s^{-1} at times reaching up to about 4–5 km s^{-1}. Most of the flows were bidirectional and similar to those associated with elongated granule-like features (EGFs) observed in the photosphere prior to Ellerman bombs (EBs) (Guglielmino et al. 2010; Yang et al. 2013, 2016; Schmieder et al. 2014). Interestingly, one end of the bidirectional flows was converging toward a point at the eastern part of the sunspot, while the other end was dispersed at the edge of the LB. In other words, the dominant direction of the horizontal flows at the edge of the LB was west. When the flow reached the edge of the LB, one of the
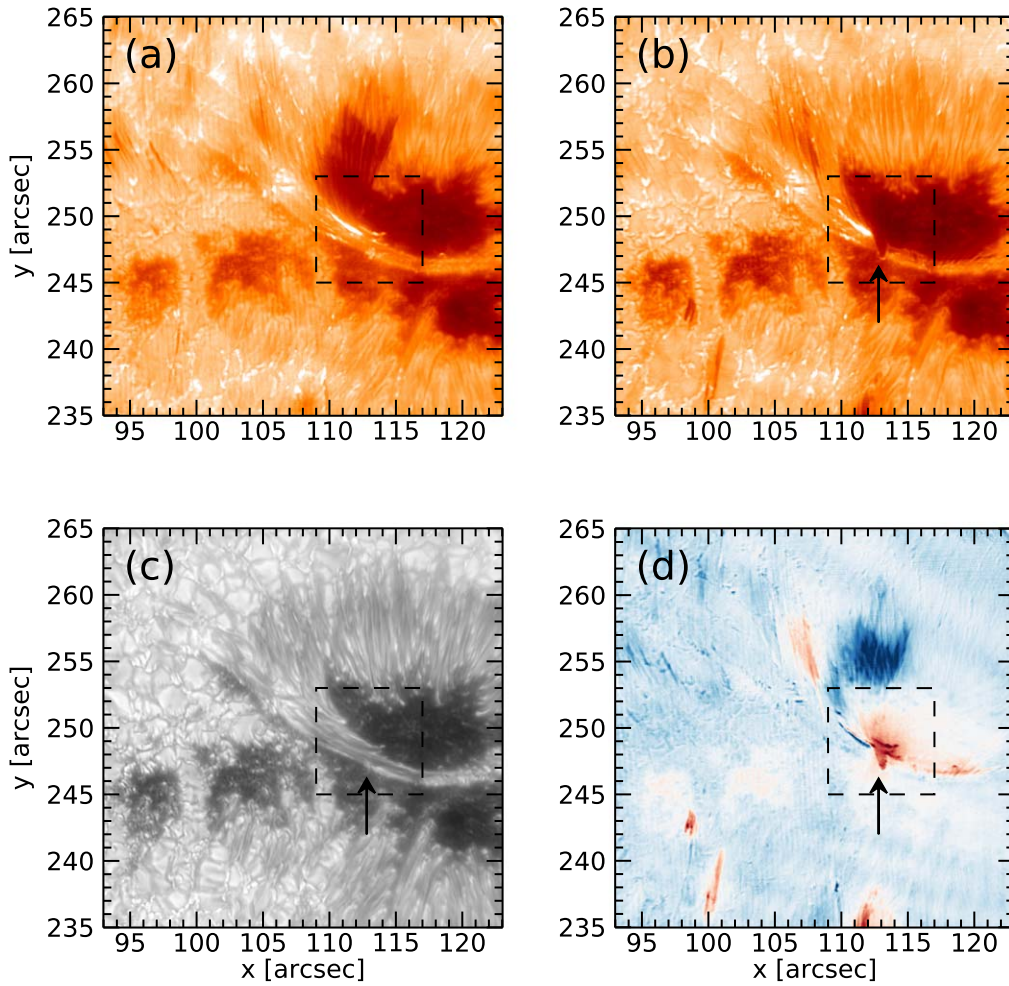
Figure 1. (a) Sunspot LB seen in the Hα wings at −0.8 Å, (b) +0.8 Å, (c) TiO, and (d) a Hα+0.8 Å Doppler map at 16:24:13 UT. The x- and y-axes indicate distance from the disk center. The dashed box represents the FOV in Figure 5. This figure is accompanied by an animation that shows the temporal evolution of the region. The video begins in the TiO filter at 16:08:42. One can see transverse flows inside the light bridge. When the flow reaches the north and south edge of the LB, one of the filaments of the LB is protruding the umbra making a curled, vortex-like shape. At 17:00:01 the video zooms in on a vortex moving ahead with the photospheric flow on the sunspot light bridge. The video continues in the TiO filter until 18:02:43 when the filter changes to the Hα wings at +0.8 Å until 18:17:43. 26 s into the video, when it begins to cycle between a single frame from the Hα wings at +0.8 Å, Hα wings at −0.8 Å, composite Hα wings at ±0.8 Å, TiO, and finally back to Hα wings at +0.8 Å. The sequence resumes 44 s in Hα wings at +0.8 Å and runs until 18:38.59. At the 18:41:33 the Hα wings at the ±0.8 Å filter are shown as the animation pans outward. The video ends at 19:59:01. Its total duration is 1 minute.

(An animation of this figure is available.)
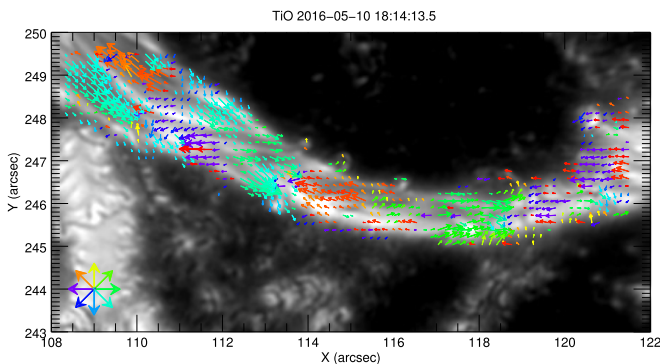
Figure 2. Velocity vectors measured using the NAVE method superposed on a TiO image. The color and the length of each arrow represent the direction and the speed of the flow, respectively. The length of the reference arrows corresponds to 3 km s^{-1}. Velocities lower than 0.2 km s^{-1}, typically found inside the umbra, were not displayed here.

filaments of the LB began to protrude into the umbral region. The maximum horizontal speed of the flow along the LB at (113″0, 246″4) was 3.4 km s^{-1}, which is much faster than the surrounding flows.

The protruding feature further assumed a curled, vortex-like shape, rolling up as it moved further into the umbra (Figure 3). As it formed, the tip of the vortex became bright in the TiO images as compared to the ambient LB region. It later became fainter after remaining at the same location for about 30 minutes.

Figure 4 shows the formation of another vortex at the north side of the LB, which followed a similar evolutionary path. A bright feature first protruded from the LB when the flow reached the edge of it and then developed into a half turned vortex, which exhibited several substructures, or secondary vortices (marked with white arrows). This is a notable development since a vortex containing secondary vortices in
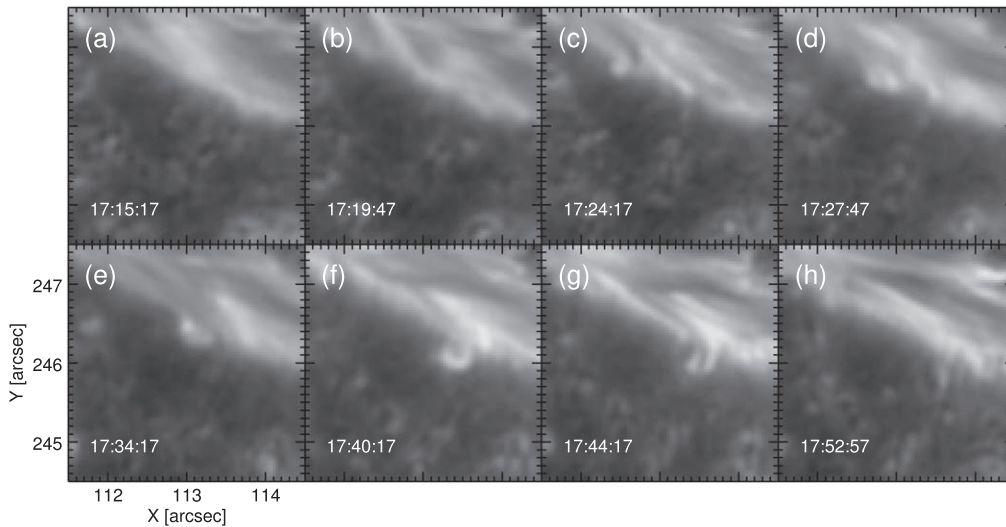
Figure 3. Formation of a photospheric vortex as a result of intrusion of an LB filament into the umbral region observed in the TiO broadband images.
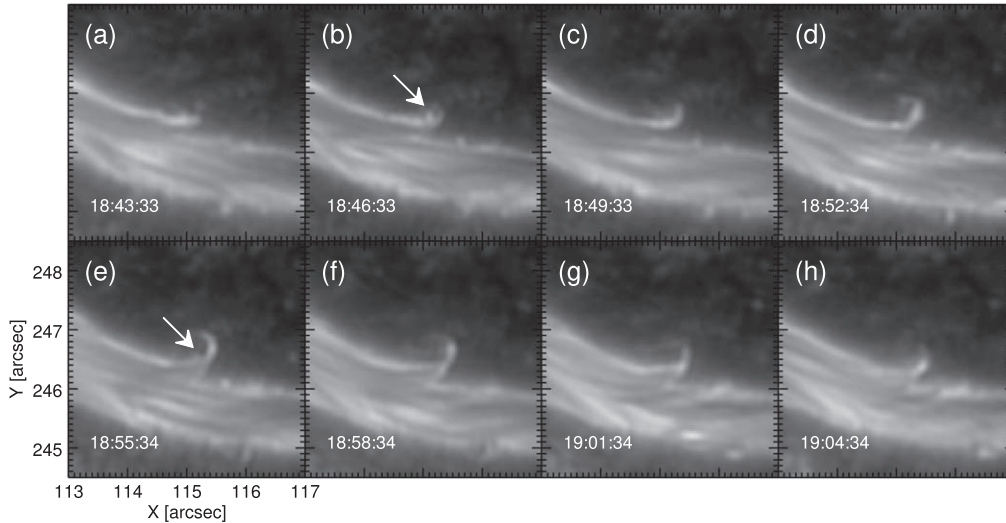
Figure 4. Formation of a filamentary vortex observed in the TiO broadband images. The white arrows represent secondary vortices when the vortex forms.

itself is expected in numerical simulations (Tian & Chen 2016; Iijima & Yokoyama 2017). In some cases the tip of the vortex detached from the main body. As in the previous vortex of Figure 3, the vortex became faint and then disappeared. But after that, it came out again when the next successive flow reached the region. As time went on, the vortex slowly moved west.

3.2. Chromospheric Surges

Chromospheric surges were observed in association with the vortex formation. Figure 5 shows six vortex events and the associated surges as they appear in the Hα $\pm$ 0.8 Å images. The surges were first observed as dark blueshifted features in the Hα line, later changing to redshifted as the ejected plasma was returning back to the chromosphere. In some instances, the position of the blue- and redshifted jets differed as shown in the fourth column in the figure. This may indicate the rotating motion of the surges (Canfield et al. 1996).

One interesting observation is that these surges appeared as a pair of narrow jets (marked with an arrow (left) in the third column of Figure 5(c). It is likely that they have a hollow tube structure so that the edge of the tube is optically thicker than the center. Sometimes, they appeared to spurt out from the photospheric vortices preserving the round shape of the vortices. Then the surges appeared to have roundish shaped tops vertical to the threads, marked by a right-hand arrow in the third column of Figure 5(c). Note that similar round and hollow jets but of a larger size were earlier observed in association with a rotating pore (Kumar et al. 2017). The cylindrical structure of the jets is expected in the numerical simulation by Iijima & Yokoyama (2017), even though their simulation was intended for quiet Sun jets.

Figures 6–8 represent the time-space (t–s) plots generated from the TiO and Hα images along the curved slits in Figures 5(a), (d), and (f), respectively (hereafter named event I, event II, event III). Note the t–s plots are of different numbers of wavelengths because the observed wavelength and the cadence of the VIS data changed during the observations. The left column in these figures represents the t–s plots along the slit. The right column shows the enlarged fraction of the t–s plots covering a 0″–2″ slit interval.

Figure 6 represents the t–s plots of event I made along the curved slits. Two surges ejected from the location of the
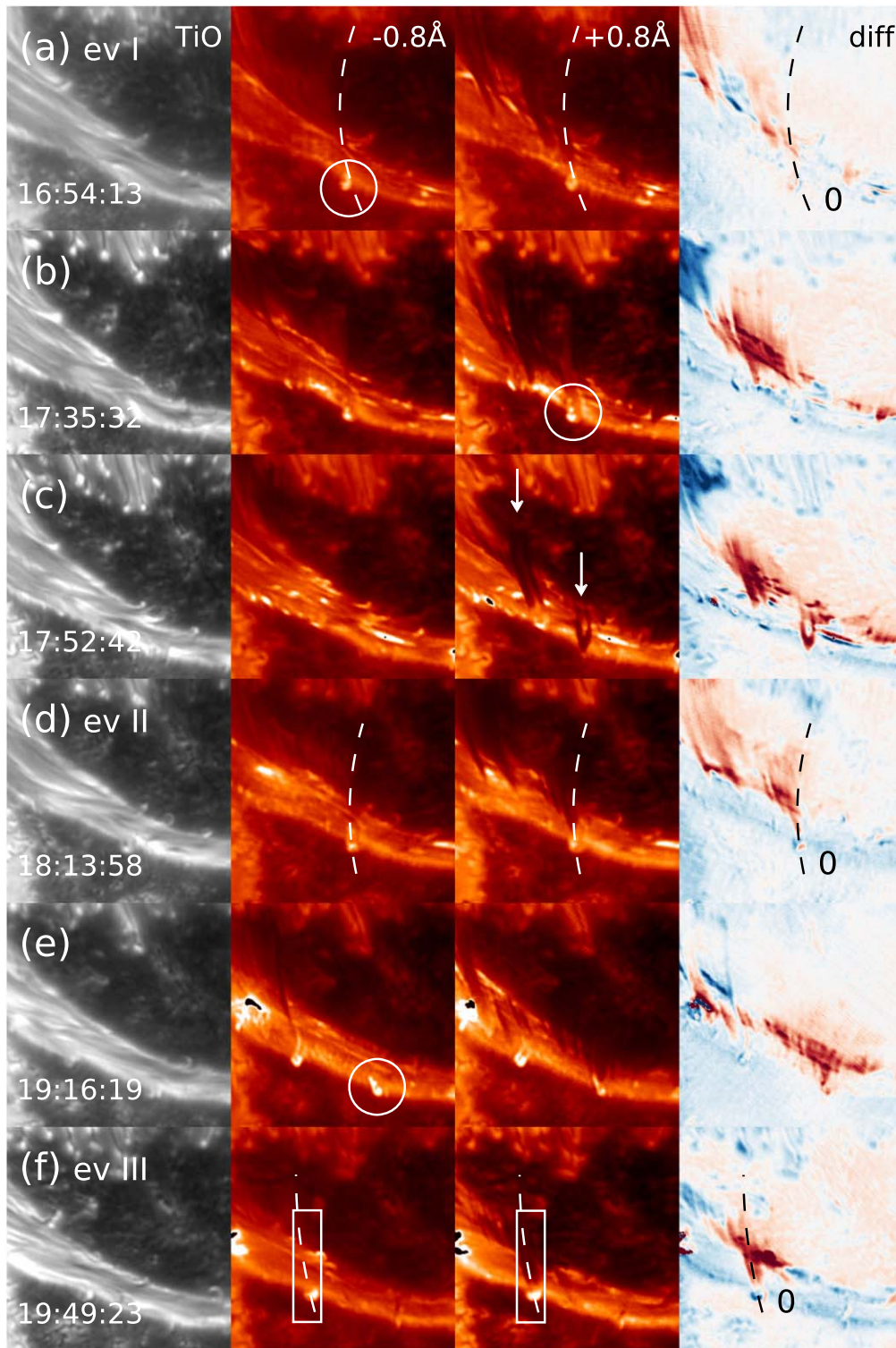
Figure 5. Six vortex events and their associated surges as seen in H$\alpha \pm 0.8$ Å images. The FOV is about 8″ by 8″ marked with the black dashed box in Figure 1. The black and white dashed lines in (a), (d), and (f) panels mark the slit position used to generate the t–s plots shown in Figures 6–8, respectively. The white circles outline the brightenings at the roots of the surges. The white arrows in the ± 0.8 Å image of (c) point to the multithreaded (hollow) flux tube structure. The white rectangles in the ± 0.8 Å image of (f) represent the FOV of Figure 9. "0" in the differential images denotes the starting point of the curved slit.

photospheric vortex at about $t = 43$ minutes and $t = 49$ minutes are marked with black arrows in (a5). The cold surge plasma is seen in absorption as dark streaks in the blue wing plots, and its spectral signature is shifted from the blue to the red wing with time, which corresponds to plasma moving along a parabolic path (Yang et al. 2013; Tian et al. 2018). The vortex

was observed from $t = 38$ minutes to $t = 51$ minutes and it is marked with a black dashed line in the TiO t–s plot of (b6). (Note that, due to the location of the slit, the vortex was recorded from about 43 to 52 minutes in the t–s plots of (a6) and (b6).) In the H$\alpha \pm 0.8$ Å, t–s plot the lower brightening is at the same location as the vortex observed between
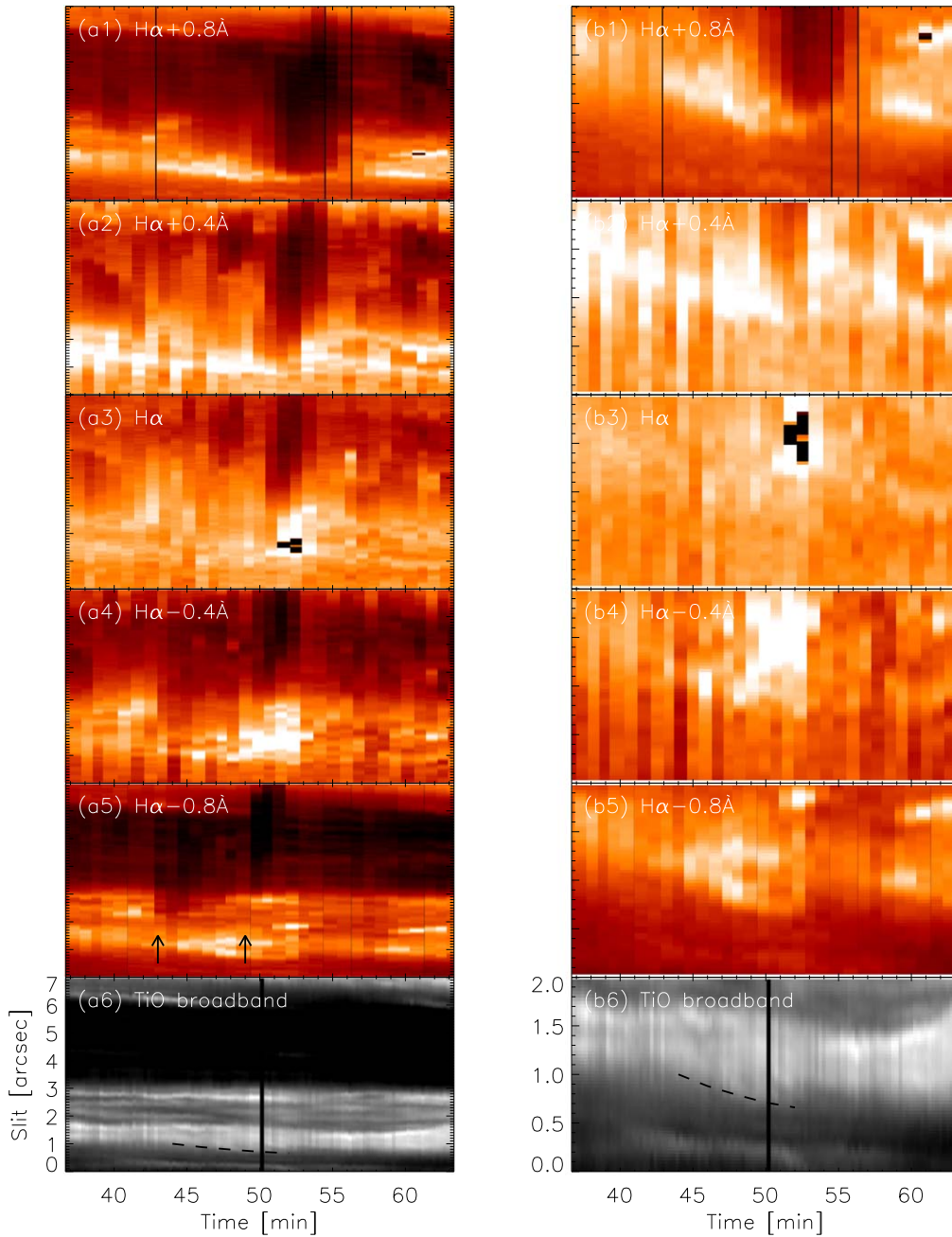
Figure 6. *t–s* plots derived from TiO and Hα data series along the curved slits shown in Figure 5(a) (left column) and enlarged *t–s* plots at *y* = 0″–2″ (right column). The black dashed lines outline the growth of a vortex. Two black arrows in (a5) mark the surges ejected from the vortex.

*t* = 43 minutes and *t* = 52 minutes. The brightenings seen in the Hα–0.4 Å and Hα line center images appear to be displaced by about 0″5–1″ as compared to those in the Hα ± 0.8 Å, images and they appeared at *t* = 47 minutes and *t* = 50 minutes, respectively. Considering that the Hα line core forms in the chromosphere and the wings form in the lower chromosphere, we speculate that the ejected plasma may have been heated in the lower chromosphere and then propelled into the corona.

Figure 7 displays a *t–s* plot of event II shown in Figure 5(b). A vortex was formed at the edge of the LB at about *t* = 123 minutes and lasted until about *t* = 135 minutes. Like the surge event I, this surge was first observed blueshifted and it later appeared redshifted. The surge appeared brighter as compared to the background intensity from *t* = 125 minutes to

t = 128 minutes (marked with white arrows in the *t–s* plot of (a3)), after then it cooled down and became dark like the other surges.

3.3. Bright Chromospheric Blobs

One of the interesting features seen in Figure 5 is Hα dynamic brightenings (blobs) observed near the roots of the surges as marked with the white solid circles in the figure. The brightenings appeared with the formation of the vortices. Their size is about 0″1–0″3 and they were often initially cospatial with the photospheric vortices seen in the TiO images. However, occasionally the bright blobs extended upward to form complex structures or multiple bright blobs.
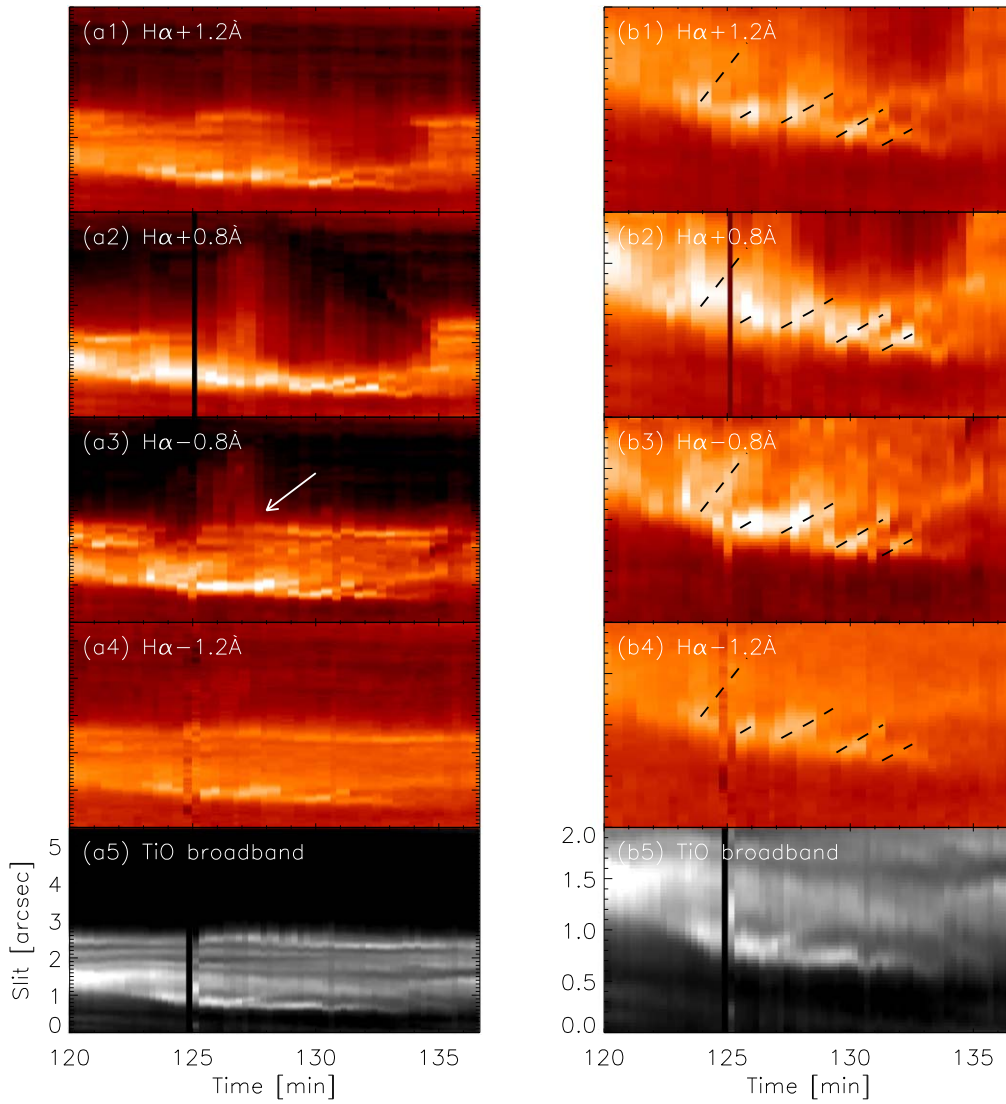
Figure 7. t–s plots derived from the TiO and Hα images along the curved slits in Figure 5(d) (left column) and enlarged t–s plots at $y = 0''$–$2''$ (right column). The black dashed lines in (b1)–(b4) represent the appearance of quasi-periodic bright blobs at the bottom of the surge. A white arrow in (a3) marks the brightenings of the surge in its early phase.

Figure 9 shows the evolution of the brightenings in the subfield of event III. The Hα brightenings were initially cospatial with the TiO vortex. Later at $t = 218.4$ minutes, one can identify a bright blob detached from the brightening and then elongated in the direction of the surge as denoted by the white circles in the figure. It appeared to be ejected from the middle of the vortex. With a size of about $0''22 \times 0''13$, it was marginally resolvable by the GST. After that, another bright blob appeared at $t = 220.7$ minutes.

In Figure 7, Hα brightenings seen at the root of the surge and consisting of multiple stripes are marked with four black dashed lines in the t–s plots of (b1) through (b4). The striped pattern represents the appearance of quasi-periodic bright blobs at the bottom of the surge during the formation of the vortex at $t = 123$–133 minutes. A total of about five propagating blobs formed near the photosphere. Their apparent speed was in the range of 1.5–$3.7\ \mathrm{km\,s^{-1}}$ and the average time gap between blobs was about 110 s.

The quasi-periodic upward motion of blobs can also be identified in Figure 8, where their trajectory is indicated with black dashed lines in the right column. In this case, the surge

itself appeared to be faint and at least four consecutive blobs were identified during the formation of the vortex between $t = 215$ minutes and $t = 222$ minutes. The apparent speeds of the blobs were in the range of 2.2–$4.1\ \mathrm{km\,s^{-1}}$. They emerged continuously during the vortex life time with a time interval of about 79 s and became fainter as they propagated upward. Note that the time resolution in Figure 8 is better than that in Figure 7 so that the motion of the bright blob is well pronounced in this case.

3.4. Magnetic Configurations and the Line-of-sight (LOS) Velocity in the Photosphere

Figures 10(a)–(d) display the NIRIS maps at a moment of event III. The magnetic field of the LB consists of a weak LOS component and a rather strong horizontal field as compared to the umbral region. At the edge of the LB the horizontal magnetic field is reversed and the LOS velocity indicates downflow, which is consistent with previous studies (Shimizu et al. 2009; Toriumi et al. 2015b). These signatures may represent a cusp shaped current layer fanning over the LB as
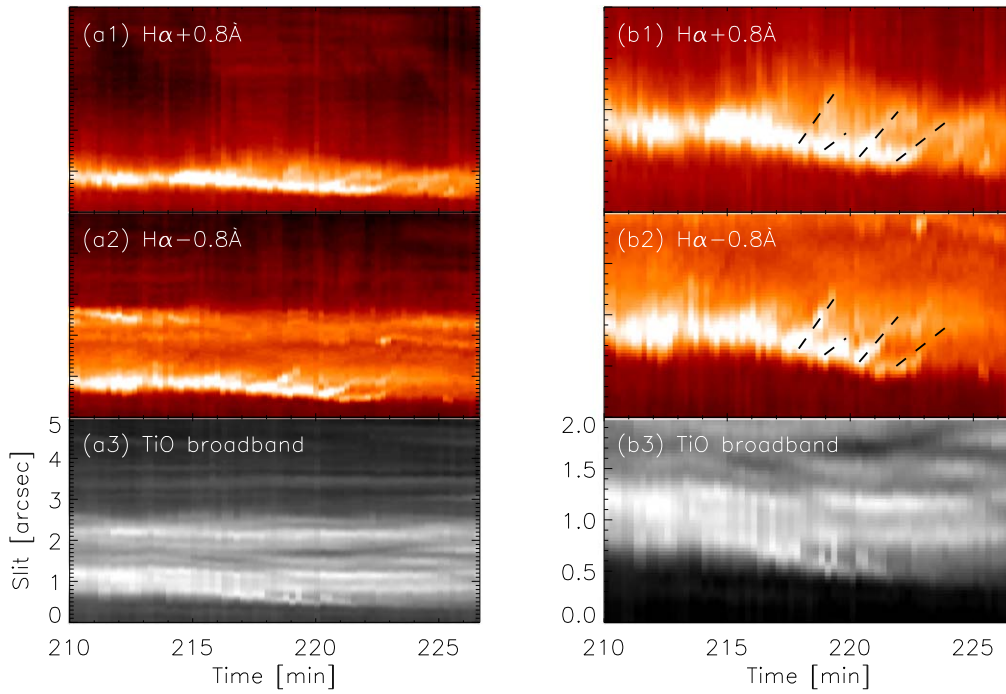
Figure 8. *t–s* plots derived from the TiO and Hα images along the curved slits in Figure 5(f) (left column) and enlarged *t–s* plots at $y = 0''–2''$ (right column). The black dashed lines in (b1)–(b2) mark the quasi-periodic bright blobs from the location of a vortex.
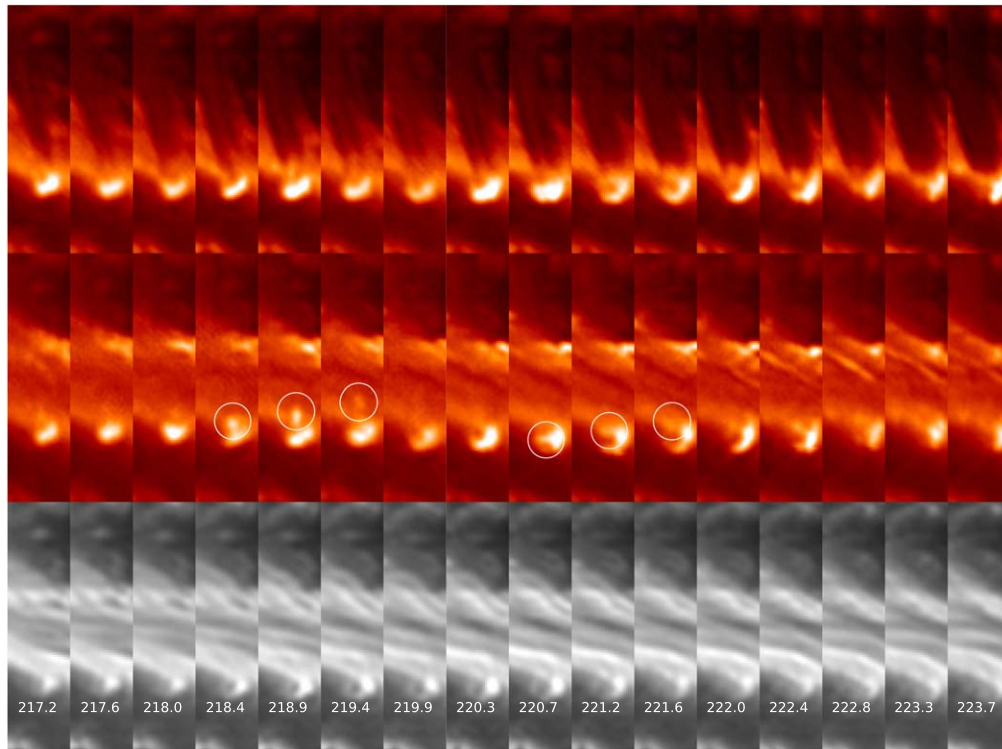

Figure 9. Evolution of the brightenings at the subfield of Figure 5(f). White circles outline two bright blobs ejected sequentially from the middle of the vortex. The FOV is $1'' \times 6''$.

well as the sinking of plasma due to magnetoconvection in the LB (Toriumi et al. 2015a). The magnetic cusp can trap emerging flux tubes in the lower chromosphere of an LB, thus causing the filamentary structures visible inside the LB.

At the site of the vortices, the horizontal and LOS magnetic field of the LB are likely to extend to the umbral region as marked with black and white ellipses in the *t–s* plots of

Figures 10(e)–(f). A strong downflow also started with the onset of the formation of a TiO vortex. From these results, we conjecture that one of the footpoints of the emerging flux, producing the strong velocity shear at the edge of the LB, may protrude into the umbra and create a vortex. Then strong downflows may be initiated following the magnetic field lines. This magnetic configuration and the velocity pattern seem to
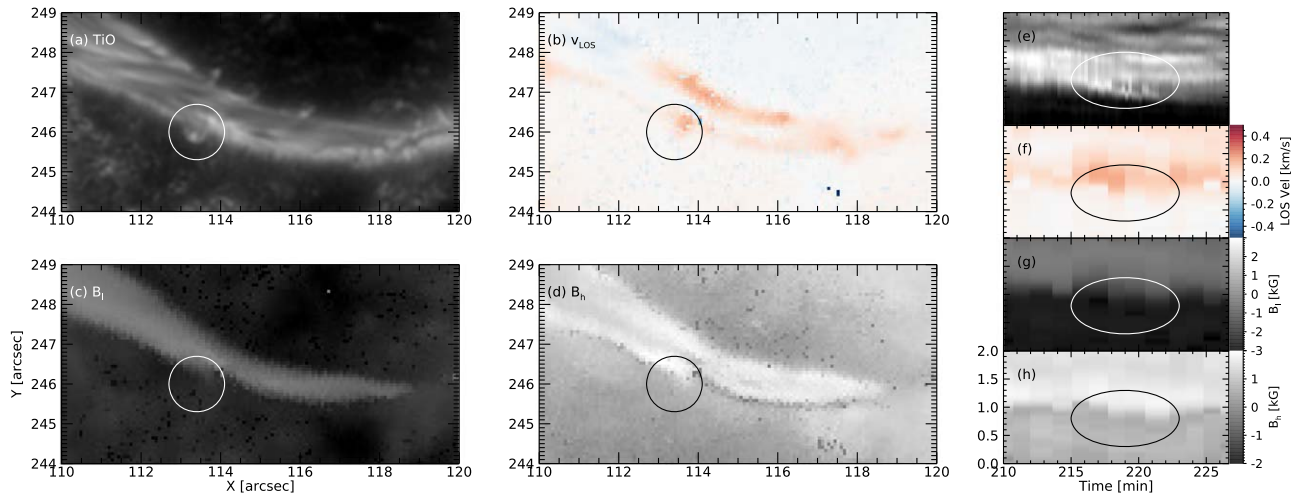
Figure 10. (a) TiO broadband photospheric image and (b) NIRIS LOS velocity, (c) transverse magnetic field and (d) LOS magnetic field maps at a moment of event III. The black and white circles represent the site of the vortices. (e) t–s plots of TiO brightening, (f) LOS velocity, (g) NIRIS LOS, and (h) horizontal magnetic field strength are derived along the same curved slits of Figure 5(f). The white and black ellipses in the t–s plots outline the appearance of the vortex.
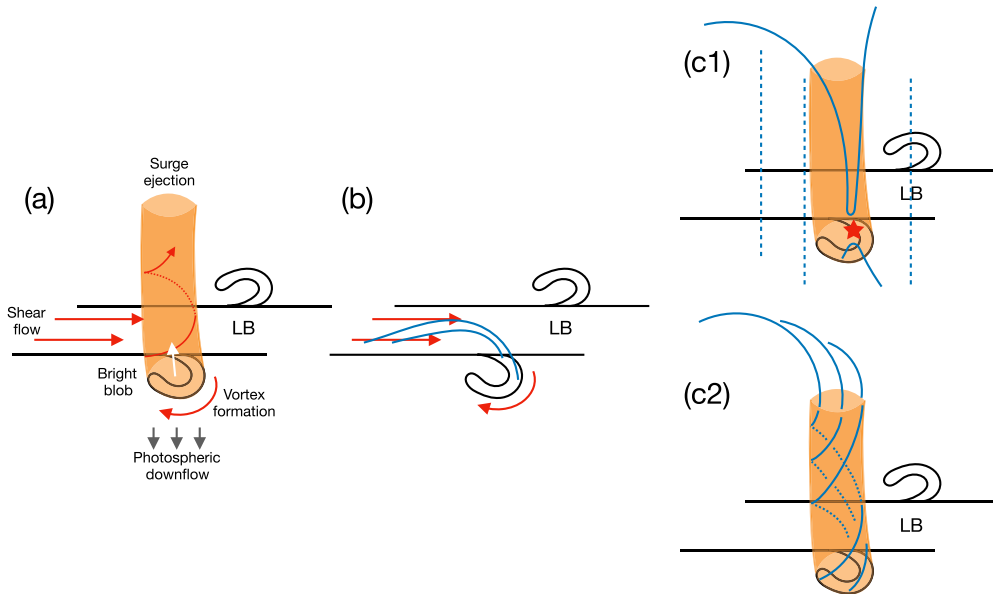
Figure 11. (a) Schematic sketch showing our observational facts, (b) a possible scenario explaining a vortex formation, (c1) a formation mechanism of a surge by magnetic reconnection between newly emerged field lines and preexisting vertical fields, or (c2) by torsional waves or twists of magnetic field lines. Red solid lines in panel (a) represent photospheric flows and surge ejection, gray arrows represent photospheric downflow, and white arrows represent bright blob motions, respectively. Blue solid lines mark the magnetic field lines. Blue dashed lines in (c1) denote the preexisting field lines in the umbral region.

resemble the magnetoconvection pattern that develops within the cusp structure of an LB (Toriumi et al. 2015b).

4. Discussion

One of the most outstanding results of the present study is the finding of photospheric vortices formed at the edge of the LB, and the accompanying surges observed in Hα images. The vortices are associated with the fast transverse motions in the photosphere. Some of the observed vortices exhibited finer, secondary vortices within them, which may be associated with the multithreaded nature of the surges (Iijima & Yokoyama 2017). When a vortex forms, photospheric horizontal and the LOS magnetic field at the edge of the LB extends to the umbral region. Strong photospheric downflows are found, too. This suggests that the vortex may be formed by the strong velocity shear produced by the emerging

flux. Each vortex was accompanied by a dark Hα surge. Those surges tended to be in a hollow cylindrical structure with bright blobs moving quasi-periodically with periods of 79 and 110 s upward along the surge spines. These observed phenomenon are illustrated in Figure 11(a). Robustini et al. (2016) showed that some chromospheric jets may be associated with finely structured photospheric features that exist at the edge of an LB but their image resolution was not high enough to identify the vortices (see Figure 1 of Robustini et al. 2016).

How are these vortices formed? We consider that the strong transverse velocity shear between the LB and the umbral region may trigger the KHI resulting in the appearance of vortex structures (see Figure 11(b)). The vortices rolled up in the clockwise direction at the southern edge of the LB, and counterclockwise in the northern edge, which can be explained by the velocity shear, and the KHI might be strongly associated

with the formation of the vortices. We, however, note that the transverse magnetic field is also enhanced at the time of vorticity formation. When the field strength reaches some threshold, the magnetic tension in the vortex boundary may be sufficient to stabilize it (Frank et al. 1996).

The vortices formed by the KHI can be strengthened by the bathtub effect. Initially weak vortices may develop due to the pressure imbalance caused by the fast magnetoconvective downflows, gathering the surrounding angular momentum, reminiscent of "inverted tornados." If the velocity shear near the edge of the LB supplies large angular momentum, the bathtub effect can strengthen the vortices more efficiently in the LB than in the quiet Sun cases. The radiative magnetohydro-dynamic simulations performed by Moll et al. (2011) show that this process can happen even with the strong magnetic field. This idea is supported by the fact that the vortices are observed in the photospheric downflowing region, where they might be formed by the downdraft plasma following the emerging magnetic flux tubes.

What, then, is the triggering mechanism of the surges? The 5–15 Mm surges ejected at the east side of the LB (see, for more details, Lim et al. 2019, in preparation), are likely to be explained by a magnetic reconnection scenario where they may be accelerated via the slingshot effect, or slow mode shock waves colliding with the transition region. As the apparent length of the surges studied in this paper was about 5 Mm, they can also be explained by small-scale magnetic reconnection as shown in Figure 11(c1). Magnetic reconnection taking place right above the vortex represented by bright upward propagat-ing blobs (Ni et al. 2015), can release the magnetic helicity to the upper atmosphere (Pariat et al. 2009). The nonlinear torsional Aflvénic waves may play a role to accelerate the plasma (Pariat et al. 2009).

Another possible mechanism of observed surges is that the surge plasma can be accelerated by nonlinear waves developing from the acoustic or Alfvén waves, not by magnetic reconnection. The waves can be produced by the photospheric vortices (see Figure 11(c2)). The surges were strongly associated with photospheric transverse flows in our observa-tion. The magnetic field rooted in the photosphere can make a vertically oriented magnetized vortex tube following the photospheric vortex formation (Kitiashvili et al. 2013). The enhancement of the gas and magnetic pressure near the root of the vortex tube will generate the acoustic shocks squeezing out the plasma into the corona. The untwisting motion of the twisted vortex tubes can also produce the torsional Alfvénic waves. The Alfvénic waves can be amplified as traveling along the stratified medium and they may generate surges.
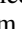
The quasi-periodic occurrence of the blobs in this paper might be due to magnetic reconnection modulated by the pulsating behavior in the reconnection site (Lee et al. 2006; Pariat et al. 2010). The periodic turbulent motions in the photosphere can also trigger magnetized quasi-periodic jets, such as spicules, tornadoes, and various surges (Kitiashvili et al. 2013; Iijima & Yokoyama 2017).

In the end, the mechanism for surge ejection should be related to the vortex formation mechanism, in addition to the magnetic field configuration. At present, there is no theoretical model that addresses both processes, as fine scale vorticity formation was rarely observed. We hope that our data and analysis of the photospheric vortices formed at the edge of the LB in the presence of fast transverse motions will prompt

further efforts to explore the origin of vorticity formation and its possible relationship with the twisted structure of surges.

ORCID iDs

Heesu Yang ⓘ https://orcid.org/0000-0001-5455-2546
Eun-Kyung Lim ⓘ https://orcid.org/0000-0002-7358-9827
Haruhisa Iijima ⓘ https://orcid.org/0000-0002-1007-181X
Vasyl Yurchyshyn ⓘ https://orcid.org/0000-0001-9982-2175
Kyung-Suk Cho ⓘ https://orcid.org/0000-0003-2161-9606
Jeongwoo Lee ⓘ https://orcid.org/0000-0002-5865-7924
Brigitte Schmieder ⓘ https://orcid.org/0000-0003-3364-9183
Yeon-Han Kim ⓘ https://orcid.org/0000-0001-5900-6237
Sujin Kim ⓘ https://orcid.org/0000-0002-5004-7734
Su-Chan Bong ⓘ https://orcid.org/0000-0003-1859-0515

References

Alexander, D., & Fletcher, L. 1999, SoPh, 190, 167
Asai, A., Ishii, T. T., & Kurokawa, H. 2001, ApJL, 555, L65
Canfield, R. C., Reardon, K. P., Leka, K. D., et al. 1996, ApJ, 464, 1016
Cao, W., Goode, P. R., Ahn, K., et al. 2012, in ASP Conf. Ser. 463, Second ATST-EAST Meeting: Magnetic Fields from the Photosphere to the Corona., ed. T. R. Rimmele et al. (San Francisco, CA: ASP), 291
Chae, J.-C., Qiu, J., Wang, H., & Goode, P. R. 1999, ApJL, 513, L75
Chae, J.-C., & Sakurai, T. 2008, ApJ, 689, 593
Cho, K.-S., Cho, I.-H., Nakariakov, V. M., et al. 2019, ApJL, 877, L1
Curdt, W., Tian, H., & Kamio, S. 2012, SoPh, 280, 417
Frank, A., Jones, T. W., Ryu, D., & Gaalaas, J. B. 1996, ApJ, 460, 777
Guglielmino, S. L., Bellot Rubio, L. R., Zuccarello, F., et al. 2010, ApJ, 724, 1083
Guglielmino, S. L., Romano, P., & Zuccarello, F. 2017, ApJL, 846, 0
Heyvaerts, J., Priest, E. R., & Rust, D. M. 1977, ApJ, 216, 123
Hollweg, J. V., Jackson, S., & Galloway, D. 1982, SoPh, 75, 35
Iijima, H., & Yokoyama, T. 2017, ApJ, 848, 0
Jiang, Y. C., Chen, H. D., Li, K. J., Shen, Y. D., & Yang, L. H. 2007, A&A, 469, 331
Kitiashvili, I. N., Kosovichev, A. G., Lele, S. K., Mansour, N. N., & Wray, A. A. 2013, ApJ, 770, 37
Kumar, P., Yurchyshyn, V., Cho, K.-S., & Wang, H. 2017, A&A, 603, A36
Kurokawa, H., & Kawai, G. 1993, in Proc. IAU Coll. 141, The Magnetic and Velocity Fields of Solar Active Regions, ed. H. Zirin, G. Ai, & H. Wang (San Francisco, CA: ASP), 507
Lagg, A., Solanki, S. K., van Noort, M., & Danilovic, S. 2014, A&A, 568, A60
Lee, J., Gary, D. E., & Choe, G. S. 2006, ApJ, 647, 638
Lim, E.-K., Yurchyshyn, V. B., Goode, P., & Cho, K.-S. 2013, ApJL, 769, L18
Lites, B. W., Scharmer, G. B., Berger, T. E., & Title, A. M. 2004, SoPh, 221, 65
Moll, R., Cameron, R. H., & Schüssler, M. 2011, A&A, 533, A126
Moore, R. L., Sterling, A. C., Falconer, D., & Robe, D. M. 2013, AAS/Solar Physics Division Meeting, 44, 103.04
Moreno-Insertis, F., & Galsgaard, K. 2013, ApJ, 771, 20
Ni, L., Kliem, B., Lin, J., & Wu, N. 2015, ApJ, 799, 79
Nishizuka, N., Shimizu, M., Nakamura, T., et al. 2008, ApJL, 683, L83
Nisticò, G., Bothmer, V., Patsourakos, S., & Zimbardo, G. 2009, SoPh, 259, 87
Nordlund, A. 1985, SoPh, 100, 209
Pariat, E., Antiochos, S. K., & DeVore, C. R. 2009, ApJ, 691, 61
Pariat, E., Antiochos, S. K., & DeVore, C. R. 2010, ApJ, 714, 1762
Pariat, E., Dalmasse, K., DeVore, C. R., Antiochos, S. K., & Karpen, J. T. 2015, A&A, 573, A130
Pariat, E., Dalmasse, K., DeVore, C. R., Antiochos, S. K., & Karpen, J. T. 2016, A&A, 596, A36

Pariat, E., Masson, S., & Aulanier, G. 2009, ApJ, 701, 1911
Robustini, C., Leenaarts, J., Rodriguez, J. d. l. C., & van der Voort, L. R. 2016, A&A, 590, A57
Roy, J. R. 1973, SoPh, 28, 95
Rust, D. M. 1968, in IAU Symp. 35, Structure and Development of Solar Active Regions, ed. K. O. Kiepenheuer (Cambridge: Cambridge Univ. Press), 77
Savcheva, A., Cirtain, J. W., DeLuca, E. E., & Golub, L. 2009, ApJL, 702, L32
Schmieder, B., Archontis, V., & Pariat, E. 2014, SSRv, 186, 227
Schmieder, B., Shibata, K., van Driel-Gesztelyi, L., & Freeland, S. 1995, SoPh, 156, 245
Schmieder, B., van Driel-Gesztelyi, L., Gerlei, O., & Simnett, G. M. 1993, SoPh, 146, 163
Shibata, K., Nishikawa, T., Kitai, R., & Suematsu, Y. 1982, SoPh, 77, 121
Shibata, K., & Uchida, Y. 1986, SoPh, 103, 299
Shimizu, T., Katsukawa, Y., Kubo, M., et al. 2009, ApJL, 696, L66
Shimizu, T., Shine, R. A., Title, A. M., Tarbell, T. D., & Frank, Z. 2002, ApJ, 574, 1074
Shimojo, M., Hashimoto, S., Shibata, K., et al. 1996, PASJ, 48, 123
Shimojo, M., & Shibata, K. 2000, ApJ, 542, 1100
Shimojo, M., Shibata, K., & Harvey, K. L. 1998, SoPh, 178, 379
Sobotka, M. 1997, in ASP Conf. Ser. 118, 1st Advances in Solar Physics Euroconference, Advances in Physics of Sunspots, ed. B. Schmieder, J. C. del Toro Iniesta, & M. Vazquez (San Francisco, CA: ASP), 155
Suematsu, Y. 1990, in Progress of Seismology of the Sun and Stars, Vol. 367, ed. Y. Osaki & H. Shibahashi (Berlin: Springer), 211
Suematsu, Y., Shibata, K., Neshikawa, T., & Kitai, R. 1982, SoPh, 75, 99
Takasao, S., Isobe, H., & Shibata, K. 2013, PASJ, 65, 62
Thomas, J. H., & Weiss, N. O. 2004, ARA&A, 42, 517
Tian, C., & Chen, Y. 2016, ApJ, 824, 1
Tian, H., Yurchyshyn, V., Peter, H., et al. 2018, ApJ, 854, 92
Toriumi, S., Cheung, M. C. M., & Katsukawa, Y. 2015a, ApJ, 811, 138
Toriumi, S., Katsukawa, Y., & Cheung, M. C. M. 2015b, ApJ, 811, 137
Wang, H. 1998, ApJ, 509, 461
Wedemeyer-Böhm, S., & Rouppe van der Voort, L. 2009, A&A, 507, L9
Wedemeyer-Böhm, S., Scullion, E., Steiner, O., et al. 2012, Natur, 486, 505
Wöger, F., von der Lühe, O., & Reardon, K. 2008, A&A, 488, 375
Yang, H., Chae, J.-C., Lim, E.-K., et al. 2013, SoPh, 288, 39
Yang, H., Chae, J.-C., Lim, E.-K., et al. 2014, ApJL, 790, L4
Yang, H., Chae, J.-C., Lim, E.-K., et al. 2016, ApJ, 829, 100
Yokoyama, T., & Shibata, K. 1995, Natur, 375, 42
Zuccarello, F., Guglielmino, S. L., & Romano, P. 2014, ApJ, 787, 57